

Exploiting Near-Field Dynamics with Movable Antennas to Enhance Discrete Transmissive RIS

Marjan Boloori, Chu Li, Aydin Sezgin

Department of Digital Communication Systems, Ruhr University Bochum, Germany

Email: {marjan.boloori, chu.li, aydin.sezgin}@rub.de

Abstract—The design of low complexity transceivers is crucial for the deployment of next generation wireless systems. In this work, we combine two emergent concepts of Movable antennas (MA) and transmissive reconfigurable intelligent surfaces (TRIS), which have recently emerged as promising technologies for enhancing wireless communication performance. In this paper, we propose a base station (BS) architecture that integrates a single MA with a TRIS operating in their near-field region. We address the joint optimization of MA location and the quantized TRIS phase configuration. Due to the non-convex coupling between spatial positioning and discrete phase constraints, an alternating optimization (AO) framework is developed, where the MA position is updated via gradient ascent (GA) and the TRIS phases are optimized through quantized phase alignment. Simulation results demonstrate that the proposed architecture significantly outperforms conventional BS equipped with a fixed fully-active antenna array under the same channel model and transmit power constraint. Moreover, MA repositioning effectively mitigates the performance degradation caused by discrete TRIS phase quantization in near-field propagation environments.

Index Terms—Transmissive RIS, movable antenna, near-field, discrete phase-shift quantization, cascaded path-loss.

I. INTRODUCTION

Reconfigurable intelligent surfaces (RIS) have emerged as a promising technology for sixth-generation (6G) wireless systems due to their capability to intelligently control the wireless propagation environment and enhance coverage and spectral efficiency [1], [2]. An RIS consists of a large number of passive elements that manipulate the phase and amplitude of incident electromagnetic waves, enabling constructive signal combination at desired receivers and interference suppression. Owing to this operation, RIS avoid the additional noise and self-interference typically associated with conventional relay technologies while maintaining low power consumption and implementation cost [3], [4].

RIS architectures can generally be categorized into reflective [5], [6] and transmissive [7], [8] configurations. In reflective RIS systems, both the transmitter and the receiver are located on the same side of the surface, which may introduce undesired coupling and deployment constraints. In contrast, transmissive RIS (TRIS) places the transmitter and receiver on opposite sides of the surface, enabling more

flexible propagation control and additional spatial degrees of freedom for channel shaping [9].

Unlike conventional wireless links, TRIS-assisted communication relies on a cascaded channel. The received signal propagates through the transmitter–TRIS and TRIS–receiver links, resulting in a multiplicative path-loss effect [10], [11]. This cascaded attenuation can significantly limit the achievable performance when the TRIS is located far from the transmitter. Consequently, deploying the TRIS in close proximity to the transmitter becomes an attractive architecture, as it reduces the first-hop propagation distance and enables more efficient signal shaping directly at the transmitter side. In such transmitter-oriented architectures, providing additional spatial control at the radiating element becomes particularly advantageous.

Movable antennas (MA) have recently emerged as a promising technique to realize this capability by allowing controlled repositioning of the antenna. This additional spatial flexibility enables adaptive spatial focusing and has been shown to significantly improve the received signal-to-noise ratio (SNR) under various channel conditions [12]–[14]. However, existing MA studies mainly focus on conventional wireless systems with direct links [15] or reflective RIS configurations [16], while the integration of MA with TRIS operating in the near-field regime remains largely unexplored.

Motivated by these insights, this work investigates the interaction between MA and a TRIS operating in the near-field region. In this configuration, the cascaded channel implies that the MA position directly influences the effective channel gain through the element-wise propagation distances between the MA and the TRIS. By adjusting the MA location, the spatial distribution of these distances can be favorably shaped, enabling improved coherent signal combination and partially alleviating the cascaded path-loss effect. In practical implementations, TRIS hardware typically employs discrete phase shifters with limited resolution, often in the range of 1–2 bits [17]–[19]. Such phase quantization generally limits the achievable channel gain due to imperfect phase alignment. In this work, we show that the spatial degree of freedom introduced by MA repositioning can effectively mitigate this hardware limitation. By appropriately adapting the MA position, the system can recover a significant portion of the performance loss caused by low-resolution phase control. As a result, the proposed architecture exploits the near-field propagation dynamics between the MA and the TRIS to enhance coherent signal combining, allowing the system to effectively mitigate

This work was supported in part by the German Federal Ministry of Research Technology and Space (BMFTR) in the course of the 6GEM+ Transfer Hub under grant 16KIS2411.

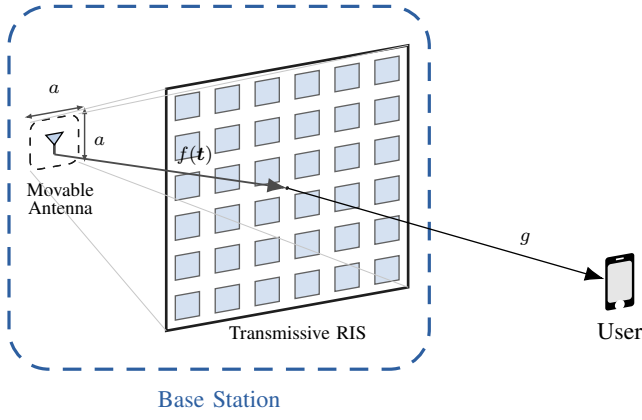


Fig. 1: System model, the suggested BS design with TRIS and MA, and the user device at the far-field.

for performance degradation caused by discrete TRIS phase quantization.

II. SYSTEM MODEL

As shown in Fig. 1, we consider a BS architecture consisting of a single MA and a TRIS. The MA is located at position $\mathbf{t} = [x_t, y_t, z_t]^T$ and can be flexibly repositioned within a two-dimensional region denoted by $\mathcal{R}_{\text{MA}} = a \times a \text{ m}^2$.

The TRIS comprises N number of transmissive elements arranged on a planar surface. The Cartesian coordinate of the n -th TRIS element is denoted by $\mathbf{e}_n = [x_n, y_n, 0]^T$, where $n \in \mathcal{N} \triangleq \{1, 2, \dots, N\}$. The inter-element spacing between adjacent TRIS elements is denoted by d_{TRIS} .

The quantized phase-shift configuration of the TRIS is represented by

$$\tilde{\boldsymbol{\phi}} = [\tilde{\phi}_1, \tilde{\phi}_2, \dots, \tilde{\phi}_n, \dots, \tilde{\phi}_N]^T, \quad (1)$$

where $\tilde{\phi}_n$ denotes the b -bit quantized phase shift assigned to the n -th transmissive element. Each discrete phase $\tilde{\phi}_n$ is obtained by mapping the corresponding continuous optimal phase ϕ_n to the nearest value in a predefined quantization set.

The TRIS is deployed in the near-field region of the MA and is assumed to be fully transmissive, meaning that the incident electromagnetic wave is transmitted through the surface without reflection. The near-field boundary, given by the Rayleigh distance, can be calculated as

$$D_{\text{Ray}} = 2D_{\text{Aper}}^2/\lambda \quad (2)$$

where λ represents the wavelength and D_{Aper} denotes the largest dimension of the TRIS [20]. In this context, $D_{\text{Aper}} = \sqrt{2N}d_{\text{TRIS}}$. This distance represents the spatial separation between the MA region and the TRIS. Subsequently, for each TRIS size, the relative Rayleigh distance for the MA is evaluated to ensure that both the MA and TRIS remain within the near-field region.

Moreover, the user is located on the opposite side of the TRIS within the far-field distance. Consequently, communication between the BS and the user is realized exclusively via a line-of-sight (LoS) link assisted by the TRIS.

Let $f_n(\mathbf{t})$ denote the near-field channel coefficient between the MA the n -th element of the TRIS which is a function of the MA position vector \mathbf{t} . The corresponding propagation distance is given by

$$d_n^{\text{T}}(\mathbf{t}) = \|\mathbf{t} - \mathbf{e}_n\|, \quad (3)$$

where \mathbf{e}_n represents the Cartesian coordinates of the n -th TRIS element. Under a spherical-wave propagation model, the resulting channel coefficient can be expressed as

$$f_n(\mathbf{t}) = \sqrt{\frac{\lambda G_f F_f}{4\pi}} \frac{1}{d_n^{\text{T}}(\mathbf{t})} e^{-j\frac{2\pi}{\lambda} d_n^{\text{T}}(\mathbf{t})}, \quad (4)$$

where λ denotes the wavelength, and G_f and F_f represent the antenna gain and the normalized power radiation pattern of the TRIS side facing the MA, respectively [21].

Similarly, the propagation distance between the n -th TRIS element and the user located at \mathbf{u} is given by

$$d_n^{\text{R}} = \|\mathbf{u} - \mathbf{e}_n\|. \quad (5)$$

Accordingly, the corresponding channel coefficient is expressed as

$$g_n = \sqrt{\frac{\lambda G_g F_g}{4\pi}} \frac{1}{d_n^{\text{R}}} e^{-j\frac{2\pi}{\lambda} d_n^{\text{R}}}, \quad (6)$$

where G_g and F_g denote the antenna gain and the normalized power radiation pattern of the TRIS side facing the user, respectively.

Based on (4) and (6), the received signal by the user can be modeled as

$$y = \sqrt{P} \sum_{n=1}^N f_n g_n \Gamma e^{j\tilde{\phi}_n} s + n_0 \quad (7)$$

where P represents the transmit power, $n_0 \sim \mathcal{CN}(0, \sigma^2)$ denotes the additive Gaussian noise with variance σ^2 , s is the transmit signal, $\Gamma \in [0, 1]$ is the transmission loss of the TRIS. Therefore, the corresponding received SNR is given by

$$\text{SNR}(\mathbf{t}, \tilde{\boldsymbol{\phi}}) = \kappa \left| c(\mathbf{t}, \tilde{\boldsymbol{\phi}}) \right|^2, \quad (8)$$

where

$$\kappa = \frac{\lambda^2 \Gamma^2 P G F}{16\pi^2 \sigma^2}, \quad (9)$$

with $G = G_f G_g$, and $F = F_f F_g$. The function $c(\mathbf{t}, \tilde{\boldsymbol{\phi}})$ is defined as

$$c(\mathbf{t}, \tilde{\boldsymbol{\phi}}) = \sum_{n=1}^N \frac{1}{d_n^{\text{T}}(\mathbf{t}) d_n^{\text{R}}} e^{j\psi_n(\mathbf{t})}, \quad (10)$$

with $\psi_n(\mathbf{t}) = \tilde{\phi}_n - \frac{2\pi}{\lambda} (d_n^{\text{T}}(\mathbf{t}) + d_n^{\text{R}})$. This function represents the cascaded MA-TRIS-user channel obtained by summing the contributions of all N TRIS elements. The phase term $\psi_n(\mathbf{t})$ denotes the effective phase of the n -th path, which consists of the applied TRIS phase shift $\tilde{\phi}_n$ and the propagation-induced phase shift determined by the total distance.

Remark 1. To assess the impact of the MA, we evaluate (8) for both discrete and continuous TRIS phase configurations. In the ideal case with continuous phase-shifters, each TRIS

element can achieve exact phase alignment with the desired transmission direction, eliminating residual phase mismatch. In other words, for any value of $\frac{2\pi}{\lambda}(d_n^T(\mathbf{t}) + d_n^R)$, the phase ϕ_n can be chosen to perfectly compensate the propagation-induced phase. In this scenario, coherent signal combining is fully achieved through phase control, and the received SNR reaches its maximum value. The resulting performance therefore serves as an upper bound for systems employing practical discrete phase-shifters. The MA position still affects the propagation distances, but perfect phase alignment ensures that the achievable SNR represents the theoretical upper bound.

$$\text{SNR}_{\text{UB}} = \kappa \left| \sum_{n=1}^N \frac{1}{d_n^T d_n^R} \right|^2 \quad (11)$$

III. PROBLEM FORMULATION AND PROPOSED ALGORITHM

In this section we concentrate on the practically relevant case of discrete phase-shifters, which also reflects typical real-world hardware and cost constraints. The goal is now to maximize the SNR in (8) by optimizing the MA location and the discrete phase-shifters of the TRIS.

The optimization problem can be formulated as

$$\mathcal{P}_1 : \quad \max_{\mathbf{t}, \tilde{\phi}} \quad \text{SNR}(\mathbf{t}, \tilde{\phi}), \quad (12a)$$

$$\text{s.t.} \quad \mathbf{t} \in \mathcal{R}_{\text{MA}}, \quad (12b)$$

$$|\tilde{\phi}_n| = 1, \quad \forall n \in \mathcal{N} \quad (12c)$$

$$\arg(\tilde{\phi}_n) \in \Phi_b, \quad \forall n \in \mathcal{N} \quad (12d)$$

where (12b) defines the two dimensional feasible region for antenna movement represented by \mathcal{R}_{MA} . The (12c) describes the constraint of the TRIS phase-shifters, and the (12d) ensures that the discrete phase-shifters are inside the defined feasible set denoted by Φ_b .

However, the optimization problem (12a) is a non-convex problem due to the discrete phase constraints and the nonlinear coupling between \mathbf{t} and $\tilde{\phi}$. To tackle this challenge, we employ an alternating optimization (AO) framework, which decouples the decision variables $\tilde{\phi}$ and \mathbf{t} in \mathcal{P}_1 by decomposing the original problem into two subproblems, where each variable is iteratively optimized while keeping the other fixed. These subproblems are solved in an alternating fashion until convergence.

A. Optimizing the MA position vector \mathbf{t}

To determine the optimal location for the MA, we implement a gradient ascent (GA) approach. The calculated gradient value of $\text{SNR}(\mathbf{t}, \tilde{\phi})$ with respect to \mathbf{t} is expressed as

$$\begin{aligned} \nabla_{\mathbf{t}} \text{SNR}(\mathbf{t}, \tilde{\phi}) = & \\ 2\kappa \Re \left\{ \left(- \sum_{n=1}^N \frac{e^{j\psi(\mathbf{t})}(\mathbf{t} - \mathbf{e}_n)}{d_n^R d_n^T(\mathbf{t})^2} \left(j \frac{2\pi}{\lambda} + \frac{1}{d_n^T(\mathbf{t})} \right) \right) c^*(\mathbf{t}, \tilde{\phi}) \right\}. & \end{aligned} \quad (13)$$

Algorithm 1 AO Algorithm for Joint Optimization of \mathbf{t} and $\tilde{\phi}$

- 1: **Initialize:** $\mathbf{t}^{(0)}$, $\tilde{\phi}^{(0)}$, step size μ_0 , minimum step size μ_{\min} , threshold ϵ , outer index $i = 0$, maximum outer iterations i_{\max} .
 - 2: Compute $\text{SNR}^{(0)} = \text{SNR}(\mathbf{t}^{(0)}, \tilde{\phi}^{(0)})$.
 - 3: **repeat**
 - 4: **MA position update (GA):**
 - 5: Set $q = 0$ and $\mathbf{t}^{(i,q)} = \mathbf{t}^{(0)}$
 - 6: **repeat**
 - 7: Compute $\nabla_{\mathbf{t}} \text{SNR}(\mathbf{t}^{(i,q)}, \tilde{\phi}^{(i)})$ using (13)
 - 8: $\mu \leftarrow \mu_0$
 - 9: **repeat**
 - 10: $\hat{\mathbf{t}} = \mathbf{t}^{(i,q)} + \mu \nabla_{\mathbf{t}} \text{SNR}(\mathbf{t}^{(i,q)}, \tilde{\phi}^{(i)})$
 - 11: $\mu \leftarrow \mu/2$
 - 12: **until** (12b) and $\text{SNR}(\hat{\mathbf{t}}, \tilde{\phi}^{(i)}) > \text{SNR}(\mathbf{t}^{(i,q)}, \tilde{\phi}^{(i)})$
 - 13: **or** $\mu < \mu_{\min}$
 - 13: $\mathbf{t}^{(i,q+1)} \leftarrow \hat{\mathbf{t}}$
 - 14: $q \leftarrow q + 1$
 - 15: **until** $q = q_{\max}$
 - 16: $\mathbf{t}^{(i+1)} \leftarrow \mathbf{t}^{(i,q)}$
 - 17: **TRIS phase update (quantized alignment):**
 - 18: **for** $n = 1, \dots, N$ **do**
 - 19: $\tilde{\phi}_n^{(i+1)} = Q\left(\frac{2\pi}{\lambda}(d_n^R(\mathbf{t}^{(i+1)}) + d_n^T); \Phi_b\right)$
 - 20: **end for**
 - 21: $\tilde{\phi}^{(i+1)} \leftarrow [\tilde{\phi}_1^{(i+1)}, \dots, \tilde{\phi}_N^{(i+1)}]^T$
 - 22: Compute $\text{SNR}^{(i+1)} = \text{SNR}(\mathbf{t}^{(i+1)}, \tilde{\phi}^{(i+1)})$
 - 23: $i \leftarrow i + 1$
 - 24: **until** $|\text{SNR}^{(i)} - \text{SNR}^{(i-1)}| \leq \epsilon$ or $i = i_{\max}$
 - 25: **Output:** $\mathbf{t}^* = \mathbf{t}^{(i)}$, $\tilde{\phi}^* = \tilde{\phi}^{(i)}$
-

B. Optimizing the TRIS phase-shift vector $\tilde{\phi}$

When employing a TRIS with discrete phase-shift adjustment, the limited resolution of the phase-shifters must be considered. Let b denote the number of quantization bits. The feasible phase set is

$$\Phi_b = \left\{ 0, \frac{1}{2^{b-1}}\pi, \dots, \frac{2^b - 1}{2^{b-1}}\pi \right\}. \quad (14)$$

We define $Q(\cdot)$ as the *quantization function*, which projects the ideal phase-shift onto the nearest element of the feasible phase set Φ_b associated with the TRIS phase-shifters

$$\tilde{\phi}_n = Q(\phi_n; \Phi_b) = \arg \min_{\phi_b \in \Phi_b} |\phi_n - \phi_b|. \quad (15)$$

As a result, each element of the quantized phase-shifter vector $\tilde{\phi}$ is calculated as

$$\tilde{\phi}_n = Q\left(\frac{2\pi}{\lambda}(d_n^R + d_n^T); \Phi_b\right). \quad (16)$$

C. Convergence and Complexity Analysis

The corresponding algorithm to optimize $\tilde{\phi}$ and \mathbf{t} is given in Algorithm 1. The algorithm follows an AO framework, where the MA position is updated via GA with backtracking and the TRIS phase vector is updated by element-wise quantized phase

alignment. Due to the backtracking rule, each accepted MA update yields a non-decreasing SNR, while the TRIS phase update maximizes coherent combining under the discrete constraint. Since the SNR is upper bounded over the feasible MA region and the finite phase set, the sequence $\{\text{SNR}^{(i)}\}$ is bounded and convergent. However, due to the non-convex nature of the problem, the algorithm converges in general to a local stationary solution. Regarding complexity, each gradient computation and SNR evaluation requires $\mathcal{O}(N)$ operations, where N is the number of TRIS elements. Hence, the overall complexity scales linearly with N , i.e., $\mathcal{O}(i_{\max}q_{\max}N)$.

IV. SIMULATION RESULTS

In this section, simulations are presented to illustrate the effects of employing a MA under a discrete phase-shifter TRIS condition. We assume the carrier frequency $f = 20$ GHz and TRIS element spacing of $\lambda/2$ and the noise variance $\sigma^2 = -90$ dBm. The user is located at a distance of 10 m of the TRIS.

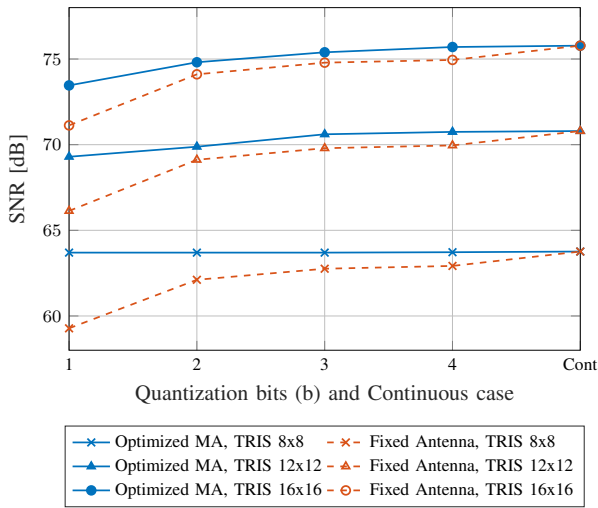


Fig. 2: SNR vs. Quantization levels for an optimized MA and a fixed position antenna.

Building on the previous results, Fig. 2 illustrates the impact of phase quantization resolution on the achievable SNR for different TRIS sizes. We consider a transmit power of $P = 13.6$ dBm and a distance of 0.5 m between the MA and the TRIS. As the number of quantization bits b increases, the SNR improves and gradually approaches the continuous-phase upper bound, since a higher phase resolution enables more accurate phase alignment across the TRIS elements. Furthermore, optimizing the MA position consistently provides an SNR gain over the fixed-antenna case for all quantization levels and TRIS sizes. This shows that the additional spatial degree of freedom introduced by the MA can partially mitigate the performance degradation caused by phase quantization. However, the remaining gap to the continuous-phase benchmark indicates that MA repositioning cannot completely remove the quantization loss. It can also be observed that this mitigation effect is relatively more pronounced for smaller TRIS sizes.

In this case, the quantization-induced mismatch is less severe and can be more effectively compensated by adjusting the MA location. For larger TRIS apertures, the discrete phase errors accumulate over more transmissive elements, making the performance increasingly sensitive to phase resolution and reducing the relative compensation achievable by a single MA.

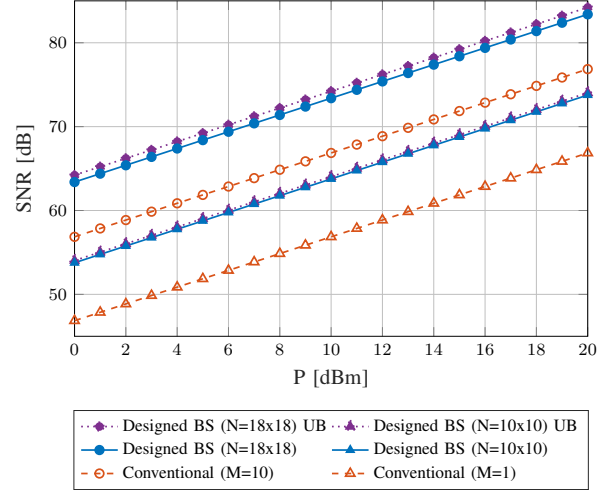


Fig. 3: Comparison of the SNR performance for the proposed BS configuration with a conventional BS.

Moreover, Fig. 3 compares the SNR performance of the proposed BS architecture with a conventional BS as a function of the transmit power constraint P . As a benchmark, we consider a conventional fully-active BS equipped with a fixed antenna array with $M \in \{1, 10\}$ number of antennas. All antenna elements are connected to dedicated RF chains and perform beamforming using maximum-ratio transmission (MRT) under the same transmit power constraint and channel model as the proposed architecture. This baseline represents the typical active antenna array employed in current wireless systems. The proposed BS consists of one MA combined with a TRIS with 2 bits quantization level and different sizes of $N \in \{10 \times 10, 18 \times 18\}$. The distance between the MA and the TRIS is 0.5 m. The case with continuous-phase TRIS elements is also shown as the upper bound. As expected, the SNR increases approximately linearly (in dB scale) with P for all configurations. The proposed BS consistently outperforms the conventional counterpart across the entire power range, and enlarging the TRIS aperture provides additional coherent combining gain.

Additionally, Fig. 4 illustrates the SNR versus P for the proposed BS architecture under near-field and far-field configurations while enforcing a constant total propagation distance $d_{\text{Tot}} = d^T + d^R = 10$ m between the MA and the user. Despite the identical total distance, a clear performance gap between the near-field and far-field regimes is observed due to the cascaded path-loss structure of the MA-TRIS-user link. Unlike direct transmission, where the received power scales with $1/d_{\text{Tot}}^2$, the TRIS-assisted link approximately follows $(\sum_n 1/(d_n^T d_n^R))^2$, resulting in product-type attenuation. In the

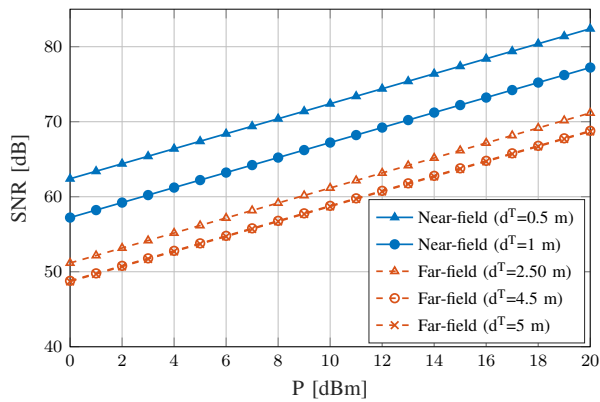


Fig. 4: SNR versus P for near-field and far-field TRIS placements.

near-field regime, the distances d_n^T vary significantly across the TRIS aperture, and some elements experience shorter propagation distances. This distance diversity improves coherent signal combining and partially mitigates the cascaded path loss. Moreover, near-field propagation enables highly localized spatial focusing, making the effective channel gain sensitive to small geometric variations between the MA and TRIS elements. In contrast, in the far-field regime the element-wise distances become nearly uniform, which reduces this effect and limits the achievable array gain. As shown in Fig. 4, increasing the MA–TRIS distance therefore causes a more pronounced SNR degradation in the near-field case, whereas the far-field performance is less sensitive due to the nearly identical propagation distances across TRIS elements.

V. CONCLUSION

In this paper, we proposed a BS architecture that integrates a MA with a TRIS operating in the near-field region. By jointly optimizing the MA position and the discrete TRIS phase-shifters through an AO framework, significant SNR gains are achieved compared to conventional BS designs. Simulation results show that the MA–TRIS architecture consistently outperforms fully-active antenna arrays under the same transmit power constraint. Furthermore, increasing the TRIS aperture size and phase resolution improves coherent combining gain and approaches the continuous-phase upper bound. These results highlight the potential of exploiting near-field propagation dynamics and antenna mobility to enhance discrete-phase TRIS-assisted wireless communication systems.

REFERENCES

- [1] Q. Wu and R. Zhang, “Towards smart and reconfigurable environment: Intelligent reflecting surface aided wireless network,” *IEEE Commun. Mag.*, vol. 58, no. 1, pp. 106–112, 2019.
- [2] Y. Liu, X. Liu, X. Mu, T. Hou, J. Xu, M. Di Renzo, and N. Al-Dhahir, “Reconfigurable intelligent surfaces: Principles and opportunities,” *IEEE Commun. Surv. Tutor.*, vol. 23, no. 3, pp. 1546–1577, 2021.
- [3] J. Zuo, Y. Liu, Z. Qin, and N. Al-Dhahir, “Resource allocation in intelligent reflecting surface assisted NOMA systems,” *IEEE Trans. Commun.*, vol. 68, no. 11, pp. 7170–7183, 2020.

- [4] W. Yan, X. Yuan, Z.-Q. He, and X. Kuai, “Passive beamforming and information transfer design for reconfigurable intelligent surfaces aided multiuser MIMO systems,” *IEEE J. Sel. Areas Commun.*, vol. 38, no. 8, pp. 1793–1808, 2020.
- [5] Z. Li, W. Chen, Q. Wu, K. Wang, and J. Li, “Joint beamforming design and power splitting optimization in IRS-assisted SWIPT NOMA networks,” *IEEE Trans. Wirel. Commun.*, vol. 21, no. 3, pp. 2019–2033, 2021.
- [6] G. Chen, Q. Wu, W. Chen, D. W. K. Ng, and L. Hanzo, “IRS-aided wireless powered MEC systems: TDMA or NOMA for computation offloading?” *IEEE Trans. Wirel. Commun.*, vol. 22, no. 2, pp. 1201–1218, 2022.
- [7] S. Zeng, H. Zhang, B. Di, Y. Tan, Z. Han, H. V. Poor, and L. Song, “Reconfigurable intelligent surfaces in 6G: Reflective, transmissive, or both?” *IEEE Commun. Lett.*, vol. 25, no. 6, pp. 2063–2067, 2021.
- [8] X. Zhu, Q. Wu, and W. Chen, “Transmissive RIS transmitter enabled spatial modulation MIMO systems,” *IEEE J. Sel. Areas Commun.*, vol. 43, no. 3, pp. 899–911, 2025.
- [9] Z. Li, W. Chen, Q. Wu, X. Zhu, H. Qin, K. Wang, and J. Li, “Toward transmissive RIS transceiver enabled uplink communication systems: Design and optimization,” *IEEE Internet Things J.*, vol. 11, no. 4, pp. 6788–6801, 2023.
- [10] S. W. Ellingson, “Path loss in reconfigurable intelligent surface-enabled channels,” in *2021 IEEE 32nd Annual International Symposium on Personal, Indoor and Mobile Radio Communications (PIMRC)*. IEEE, 2021, pp. 829–835.
- [11] S. Alfattani, W. Jaafar, Y. Hmamouche, H. Yanikomeroglu, and A. Yongaçoglu, “Link budget analysis for reconfigurable smart surfaces in aerial platforms,” *IEEE open j. Commun. Soc.*, vol. 2, pp. 1980–1995, 2021.
- [12] L. Zhu, W. Ma, and R. Zhang, “Modeling and performance analysis for movable antenna enabled wireless communications,” *IEEE Trans. Wirel. Commun.*, vol. 23, no. 6, pp. 6234–6250, 2023.
- [13] L. Zhu, W. Ma, Z. Xiao, and R. Zhang, “Performance analysis and optimization for movable antenna aided wideband communications,” *IEEE Trans. Wirel. Commun.*, 2024.
- [14] W. Ma, L. Zhu, and R. Zhang, “Movable antenna enhanced wireless sensing via antenna position optimization,” *IEEE Trans. Wirel. Commun.*, vol. 23, no. 11, pp. 16 575–16 589, 2024.
- [15] L. Zhu, W. Ma, B. Ning, and R. Zhang, “Movable-antenna enhanced multiuser communication via antenna position optimization,” *IEEE Trans. Wirel. Commun.*, vol. 23, no. 7, pp. 7214–7229, 2024.
- [16] H. Wu, H. Ren, C. Pan, and Y. Zhang, “Movable antenna-enabled RIS-aided integrated sensing and communication,” *IEEE Trans. Cogn. Commun. Netw.*, vol. 11, no. 5, pp. 2879–2892, 2025.
- [17] R. Song, H. Yin, Z. Wang, T. Yang, and X. Ren, “Modeling, design, and verification of an active transmissive RIS,” *IEEE Trans. Antennas Propag.*, 2024.
- [18] D. Shen, F. Lan, L. Wang, T. Song, M. Yang, T. Hu, Y. Li, X. Nie, J. Yang, S. Liang, H. Zeng, H. Zhang, P. Mazumder, Z. Yang, Y. Zhang, and T. Cui, “Sub-terahertz transmissive reconfigurable intelligent surface for integrated beam steering and self-OOK-modulation,” *Light Sci. Appl.*, vol. 14, 2025.
- [19] J. Tang, M. Cui, S. Xu, L. Dai, F. Yang, and M. Li, “Transmissive RIS for B5G communications: Design, prototyping, and experimental demonstrations,” *IEEE Trans. Commun.*, vol. 71, no. 11, pp. 6605–6615, 2023.
- [20] Y. Pan, C. Pan, S. Jin, and J. Wang, “RIS-aided near-field localization and channel estimation for the terahertz system,” *IEEE JSTSP*, vol. 17, no. 4, pp. 878–892, 2023.
- [21] W. Tang, M. Z. Chen, X. Chen, J. Y. Dai, Y. Han, M. Di Renzo, Y. Zeng, S. Jin, Q. Cheng, and T. J. Cui, “Wireless communications with reconfigurable intelligent surface: Path loss modeling and experimental measurement,” *IEEE Trans. Wirel. Commun.*, vol. 20, no. 1, pp. 421–439, 2020.